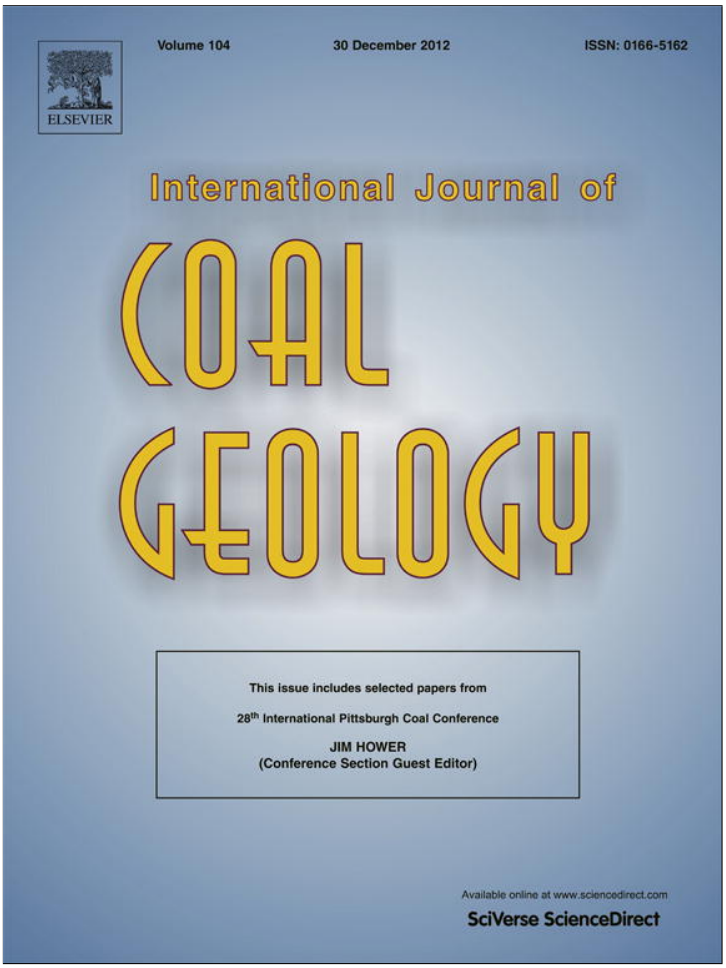

International Journal of Coal Geology 104 (2012) 83–95

Contents lists available at SciVerse ScienceDirect

International Journal of Coal Geology

journal homepage: www.elsevier.com/locate/ijcoalgeo

Molecular simulation of CO_2 adsorption in micro- and mesoporous carbons with surface heterogeneity

Yangyang Liu, Jennifer Wilcox *

Department of Energy Resources Engineering, School of Earth Sciences, Stanford University, Green Earth Sciences 065, 367 Panama Street, Stanford, CA 94305, United States

ARTICLE INFO

Article history:
Received 8 January 2012
Received in revised form 10 April 2012
Accepted 11 April 2012
Available online 20 April 2012

Keywords:
Surface heterogeneity
CO_2 adsorption
Density functional theory
Molecular simulation
CO_2 storage capacity

ABSTRACT

To mitigate and stabilize atmospheric CO_2 concentrations, alternate energy sources with zero carbon emissions offer ultimate solutions. However, technologies based on efficient and economic generation of electricity from non-carbonized energy sources are still in development. Therefore, carbon capture combined with sequestration as a component of a greater portfolio of solutions to reduce CO_2 emissions may be carried out during our transition from fossil-based resources to renewables or non-carbonized resources. As one of the attractive options, CO_2 captured by carbon-based sorbents as well as CO_2 sequestration in unmineable coalbeds require a thorough understanding of the adsorption properties in micro- and mesoporous carbon materials. An obstacle is insufficient understanding of the molecular-level mechanisms associated with CO_2 adsorption on realistic carbon pore surfaces with chemical heterogeneities and at pressures and temperatures characteristic of the depths of coal in the subsurface. Current fundamental investigations of gas adsorption onto functionalized carbon surfaces involve the characterization of carbon-based samples by experimental methods, understanding of electronic properties of functionalized carbon surfaces by density functional theory, and the thermodynamic property predictions using a Monte Carlo method within the grand canonical ensemble. With the consideration of surface chemistry, CO_2 storage capacity estimations in organic matrix of coal and gas shale increase greater than 40% when CO_2 is adsorbed in the ultramicropores, and greater than 15% in 2-nm micropores.

1. Introduction

Annual energy-related CO_2 emissions in the U.S. have reached approximately 5.6 Gt in 2010 according to the Energy Information Administration (EIA), which account for more than 80% of the nation's greenhouse gas emissions (EIA, 2012). To stabilize the atmospheric CO_2 emissions at a level that could minimize the impact on the global climate, our energy system must ultimately rely on renewable energy sources (DOE, 2010). However, technologies based on thermodynamically efficient and economically viable large-scale economic electricity generation from non-carbon-based energy sources are still in development. Therefore, CO_2 capture and sequestration (CCS) may provide a bridging strategy to the development of non-carbonized energy systems.

To determine the potential of CO_2 storage in coal and gas shale reservoirs, a thorough investigation of the mechanisms of CO_2 adsorption in complex micro- and mesoporous carbon-based materials is needed. In the case of carbon capture by carbon-based solid sorbent, although it is a separate process, at the molecular-scale, they both share a major challenge, i.e., an insufficient fundamental understanding of the density variations associated with the adsorbed phase within a given pore and among various pore diameters, leading to subsequent difficulties in predicting accurate CO_2 adsorption capacities. Thus, molecular-level simulations of carbon-based systems with surface functionalities, which can be thought to represent synthetic carbon-based sorbents and organic matter in natural materials with structural and/or chemical heterogeneities, are of interest for both carbon capture and storage applications.

Coal and the organic components of gas shale are comprised of extremely complex pore networks with varying pore size, shape, and surface functionality. To investigate the process of gas adsorption–desorption using statistical modeling, these complex pore structures of carbon-based porous materials have frequently been modeled as a collection of independent, non-interconnected slit pores with perfect graphitic walls (Bhatia et al., 2004; Hu et al., 2011; Kowalczyk et al., 2010; Kurniawan et al., 2006; Lastoskie et al., 1993; Müller, 2005; Tenney and Lastoskie, 2006; Zhu et al., 2005; etc.). However, as the disagreement between the modeling and experimental adsorption isotherms suggests, models that do not include structural and chemical heterogeneities fail to accurately predict adsorption capacities (Jorge et al., 2002; Tenney and Lastoskie, 2006). Previous experimental studies provide indication that the natural carbon-based systems include both aromatic and aliphatic structures, as well as a variety of surface functional groups (e.g. hydroxyl, carboxyl, carbonyl) (Haenel, 1992; Smith et al., 1994; van Krevelen, 1991; White et al., 2005), including volatile components such as water vapor, methane, and nitrogen- and sulfur-containing compounds. Such

* Corresponding author. Tel.: +1 650 724 9449; fax: +1 650 725 2099.
E-mail address: wilcoxj@stanford.edu (J. Wilcox).

0166-5162/$ – see front matter © 2012 Elsevier B.V. All rights reserved.
doi:10.1016/j.coal.2012.04.007

chemical heterogeneity will likely play an important role in determining the adsorption capacity and adsorbed/gas phase equilibrium properties such as density, heat of adsorption, and packing within the pore. In addition, embedded functional groups will change the electrostatic properties of the sorbent surface, and, thus, are expected to play an important role in the adsorption mechanisms associated with CO_2 in these systems depending on the temperature and pressure conditions. In the case of carbon storage, the study of surface chemical functionality is essential for the prediction of CO_2 storage capacity. Such investigations will reveal which functional groups act to passivate or enhance CO_2-surface adsorption. For example, it was observed by neutron scattering techniques that the density of adsorbed CO_2 in certain coal samples is greater in regions where the mineral matter is limited (Melnichenko et al., 2009; Radlinski et al., 2009), which indicates that surface functionalities contained in the coal samples that were investigated in this previous work hinder the CO_2 adsorption. Therefore, the inclusion of these surface functionalities in the carbon model is required to accurately determine the mechanism of adsorption and subsequent material capacity. Additionally, knowledge of the packing of CO_2 in the pore structure and the forces that underlie the existence of the condensed phase, will aid in understanding the heats of sorption associated with CO_2 in a variety of pores that differ either in size and/or in surface chemistry.

Although the adsorption of CO_2 on simplified graphitic surfaces has been experimentally and computationally investigated previously (Allouche and Ferro, 2006; Cabrera-Sanfelix, 2009; Chen and Johnson, 2005; Cinke et al., 2003; Jiang and Sandler, 2005; Matranga et al., 2003, 2004; Montoya et al., 2003; Rivera et al., 2002; Xu et al., 2006; Yim et al., 2004; Zhao et al., 2002), few statistical molecular simulations of CO_2 adsorption have taken pore surface chemical heterogeneity into account. Tenney and Lastoskie (2006) carried out molecular simulations to investigate the influence of surface heterogeneity on predicted adsorption behavior in functionalized slit-pores. Two types of heterogeneous structures were studied: the graphite edge sites with dangling bonds occupied by hydroxyl (−OH) or carboxyl (−COOH) groups, and the graphene basal plane with defects and oxygen functional groups. The force-field parameters for the various elements were either taken from the literature or calculated based on results obtained from ab initio calculations for ~100-atom polycyclic aromatic hydrocarbons at the HF/6–31 g(d,p) level of theory along with a Mulliken charge analysis. However, according to the previous experimental and theoretical work carried out by Kudin et al. (2008), hydroxyl groups do not exist at edge sites but only as active sites on the basal surface. It is crucial to investigate functional groups that reflect realistic flue gas conditions in the case of carbon capture or geologic conditions in the case of storage. Furthermore, additional oxygen-containing functional groups, such as carbonyl, epoxy, etc., which inherently exist in the structure of coal (Kudin et al., 2008; van Krevelen, 1991) have not been included in previous molecular simulation studies concerning CO_2 adsorption.

The objectives of this work are to evaluate the influence of realistic surface functional groups of carbon pore surfaces on the adsorption capacity of CO_2. Plane-wave-based electronic structure calculations were performed to determine the electronic distribution of the functionalized carbon surfaces. A Bader charge analysis was undertaken to calculate the partial charge distributions, which are required for determining the energy contributions in the statistical simulations. In particular, Monte Carlo (MC) simulations have been carried out within the Grand Canonical ensemble to predict the thermodynamic equilibrium properties of the CO_2-carbon pore system.

2. Computational methodology

2.1. Density functional theory (DFT)

Electronic structure calculations of functionalized carbon surfaces were carried out using the Vienna ab initio simulation package (VASP) (Kresse and Furthmüller, 1996; Kresse and Hafner, 1993). Plane-wave electronic density functional theory was employed due to its balanced computational efficiency and reasonable accuracy in predicting the partial charge distributions. The DFT calculations coupled with a *van der Waals*-inclusive correction (DFT-D) (Grimme, 2006) were carried out to improve the calculations of the energies associated with the interlayer interactions of graphitic structures, which is around 3.35 Å. The corresponding partial charge values associated with the top-layer atoms are compared with the values calculated from DFT without the corrections. The projector-augmented wave (PAW) potential (Kresse and Joubert, 1999; Perdew et al., 1996) was used to describe the core–valence electron interaction of the carbon and oxygen atoms. The model of Perdew, Burke, and Ernzerhof (PBE) (Perdew et al., 1996) was employed for the nonlocal corrections and an $11\times11\times1$ Monkhorst–Pack (Monkhorst and Pack, 1976) k-point sampling grid with a plane-wave cutoff of 750 eV was used. An idealized perfect and functionalized carbon-based pore surface was represented by a three-layer graphite slab. Previous investigations (Cabrera-Sanfelix, 2009; Sanfelix et al., 2003) have confirmed that three graphene layers are sufficient to model the CO_2–surface interactions within a slit pore comprised of a graphite framework due to the weak influence that the neighboring carbon layers have on the adsorption energy. Given the periodic boundary conditions, a vacuum region of 20 Å between the slabs was used to prevent interactions between the periodic images. The investigated systems include a perfect graphite basal plane surface, a hydrated graphite surface, and six oxygen-containing functionalized-graphite surfaces, each with unique vacancy sites or functional groups. Previous DFT and experimental studies have investigated similar functional groups and have shown them to be stable on graphene or graphite surfaces. In addition, these functional groups are likely to exist in coal and the organic matrix of gas shale due to the presence of water vapor and subsequent water–surface interactions (van Krevelen, 1991). As shown in Fig. 1, the graphite surface functional groups of the following types are considered: mono-vacancy (Hashimoto et al., 2004) with dissociated H_2O (Kostov et al., 2005); epoxy functionalized (Kudin et al., 2008); hydroxyl functionalized (Bagri et al., 2010; Kudin et al., 2008); carbonyl functionalized (Bagri et al., 2010); carboxyl functionalized; and combined hydroxyl–carbonyl functionalized (Bagri et al., 2010).

The investigated functional groups were positioned on either a 6×6 (e.g., hydrated graphite surface and carboxyl functionalized surface) or a 4×4 (e.g., other embedded oxygen-containing functionalized surfaces) carbon-ring unit cell with functional groups located in the center of the top graphene layer. To balance the computational time and accuracy of the calculations, all of the atoms in the top two layers were allowed full flexibility, while the positions of the carbon atoms in the bottom layer were fixed. For a fair and accurate comparison of adsorption properties among various functionalities, the O:C ratio of the functionalized surfaces with a 4×4 carbon-ring unit cell was kept as 1:24.

To investigate the relative reactivity of water vapor and CO_2 on the mono-vacancy site (Hashimoto et al., 2004) and then to determine the ultimate stable graphite surface, the dissociation of water vapor and CO_2 was investigated. The adsorption energy can be calculated from Eq. (1):

$$E_{ads} = E_{surf+CO_2/H_2O} - E_{surf} - E_{CO_2/H_2O}. \quad (1)$$

The adsorption energies were compared, with the lower energy representing the more stable surface.

Bader charge analysis (Bader, 1990) was undertaken to calculate the partial charge distributions of the perfect graphite and the functionalized graphite surfaces, which are required for the energy contributions in the statistical model simulations.

2.2. Molecular simulations

Grand canonical Monte Carlo (GCMC) simulations (Frenkel and Smit, 2002) of CO_2 adsorption in idealized organic microporous carbons were

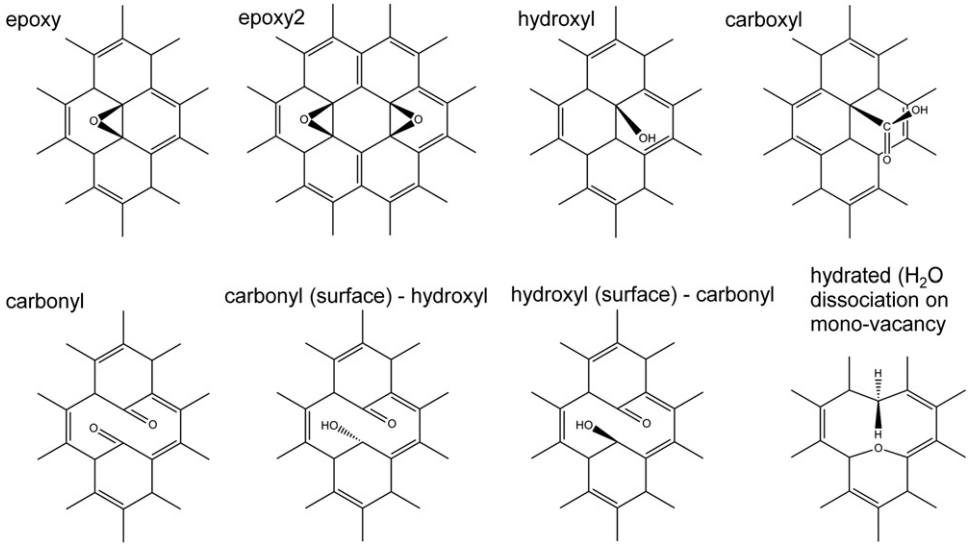

Fig. 1. Functionalized graphitic surfaces investigated in the current work. These functional groups are positioned in the center of the top layer of the periodic graphite slabs.

carried out in the μVT ensemble (Gupta et al., 2003). The Peng-Robinson equation of state was used to relate the bulk experimental pressure with the chemical potential required in the GCMC simulations. A total of approximately 100 million GCMC moves were attempted during each GCMC simulation. To reduce the computational time, a rigid graphite framework was assumed. The rigid framework assumption is based on the fact that the graphitic structures have been optimized in the plane-wave DFT calculations and that the geometries of the framework are not significantly influenced by CO_2 adsorption.

Phase properties of CO_2 are important for both transportation and storage processes. Assuming that the surface temperature (T_s) is 10 °C, the temperature gradient (dT/dz) is 30 °C/km, the density of water underground does not change as a function of depth (i.e., $\rho_w = 1000$ kg/m^3), and the surface pressure is atmosphere pressure (i.e., 0.1 MPa), the temperature and pressure increase linearly. (Benson and Cook, 2005) In the Powder River Basin, for example, coal seams are approximately 300-m deep, with corresponding temperature and pressure conditions of approximately 20 °C and 3 MPa, respectively; in shale, the Barnett gas shale reservoir is about 2-km deep, for example, and therefore the temperature and pressure are approximately 70 °C and 20 MPa, respectively. In the current work, temperature conditions of 298 K/313 K and pressure conditions up to 25 MPa were investigated, which are generally relevant to sequestration applications.

Physisorption processes of CO_2 in microporous carbons are predominantly associated with *van der Waals* forces (also known as dispersion–repulsion forces) and electrostatic forces (also known as Columbic interactions), which are sourced mainly from permanent dipole, quadrupole, and higher-induced-pole interactions. The *van der Waals* forces are present in all systems, but the electrostatic interactions are only present in systems that contain charge, such as charge due to surface functional groups or surface defects (Wilcox, 2012).

In the current work, the CO_2 molecule was represented by two potential models, e.g., the one-center Lennard–Jones model and the TraPPE model, (Potoff and Siepmann, 2001), which is a three-site rigid model that accounts for the intrinsic quadrupole moment of CO_2 using a partial charge at each site. In the case of the one-center Lennard–Jones model, CO_2 is represented by a single L–J potential site, and the LJ parameters are tuned by comparing the GCMC-predicted bulk CO_2 density to experiment measurements, as shown in Table 1. To investigate the surface functionality, the one-center Lennard–Jones model does not account for charge, and therefore the TraPPE model has been employed. The partial charges on C and O atoms are $q_C = 0.70$ e and $q_O = -0.35$ e (e $= 1.6022 \times 10^{-19}$ C), respectively. The CO_2 molecule has a C═O bond length of 1.16 Å, with an O═C═O bond angle of 180°. The CO_2–CO_2 interactions were modeled as a combination of Lennard–Jones (LJ) and Columbic potentials, where the *van der Waals* interactions between two LJ sites were calculated using the LJ 12–6 potential and the electrostatic interactions were calculated based on the Bader charge analysis. The potential energies associated with different LJ sites were calculated using standard Lorentz–Berthelot mixing rules (Allen and Tildesley, 1989). As shown in Table 1, the LJ parameters for the other species contained within the surface functional groups were taken from previous molecular simulation studies of Tenney and Lastoskie (2006).

In this work, the effects of carbon surface functionality on the adsorption of CO_2 were investigated by simulating CO_2 adsorption in idealized carbon frameworks with various embedded functional groups and surface defects, which were represented by the DFT-optimized perfect and functionalized graphitic slit pores.

Due to the potential existence of undercoordinated carbon atoms in the pore structure, the graphitic surfaces are reactive toward inherent volatile components contained in the carbon matrix, such as water vapor. In the case that temperature and pressure conditions favor surface-bound water or various forms of surface-dissociated water, the CO_2-surface adsorption may be passivated or enhanced due to the existence of oxygen-containing functional groups.

In addition, there may be inherent functional groups in the natural systems including oxygen, hydrogen, nitrogen, and sulfur atoms. As discussed in Section 2.1, the functional groups investigated in the current work include epoxy, hydroxyl, carbonyl, and carboxyl chemistries.

For both lab measurements and molecular simulations, it is essential to accurately determine the pore volume available for adsorption. Given that helium is a non-adsorbing gas (or very weakly adsorbing gas), the pore volume is typically determined using helium at ambient temperature before initiating adsorption experiments. While the pore volume accessed by helium is not necessarily the same as that by CO_2 at the same temperature and pressure conditions, the helium pore volume measurements may accurately describe the trend associated with the pore volume as it is influenced by the various functional groups. Furthermore, the helium pore volume measurements are conducted using grand canonical Monte Carlo method in this work for consistency with experimental work, in which helium pore volume measurements are widely used. The detailed algorithm associated

Table 1
Potential parameters for the force field calculations.
After Tenney and Lastoskie (2006).

		ε_{ff}/k_B [K]	σ_{ff} [Å]
1C-LJ	CO_2–CO_2	240	3.75
TraPPE	$C(CO_2)$–$C(CO_2)$	27	2.8
	$O(CO_2)$–$O(CO_2)$	79	3.05
C(graphite)–C(graphite)		28	3.4
O(surface functional groups)		79	3.1
H(surface functional groups)		30	1.31

with the pore volume calculation using helium is available in the Supplementary data.

3. Results and discussion

3.1. Study of CO_2 adsorption isotherms

The implementation of the GCMC method yields the adsorption isotherms of a given adsorbent–adsorbate interaction in micro- and meso-slit pores: the total and the excess adsorption isotherms were predicted and the effects of pore size and surface functionality have been investigated. Total adsorption represents the total amount of CO_2 adsorbed per unit pore volume, including CO_2 in both condensed surface-bound adsorbed phase and weakly surface-bound gas phases. The excess adsorption is the additional amount of CO_2 adsorbed per unit pore volume compared with the amount of CO_2 in the same volume as the pore without the pore walls. The conversion from total to excess adsorption bridges the molecular simulation results to the direct experiment measurements.

3.1.1. Comparison of adsorption capacity with pore size in micropores based upon different potential models

Two potential models of CO_2 are compared in the current work. The one-center Lennard–Jones model (1C-LJ) is computationally efficient, but less accurate, especially when the surface chemistry with heterogeneous partial charge distribution is not negligible. The TraPPE model treats CO_2 as a three-site rigid molecule and takes the intrinsic quadrupole moment of CO_2 into account through the inclusion of the partial charge at each atomic site. The TraPPE model is better at descripting vapor–liquid equilibrium, and is also more computational intensive. All of the parameters for both models are tuned by matching the simulation results of the bulk phase CO_2 isotherms with the lab measurements at the same temperature and pressure conditions.

Fig. 2 shows the comparisons of the total amount of CO_2 in the slit pores per unit volume as a function of the pore width at two different pressure conditions. In general, at low loadings, e.g., 0.2 MPa of CO_2, the adsorbate molecules tend to occupy the adsorption sites that are close to the pore walls. These sites are the most energetically-favorable positions in the pore where the energy associated with the CO_2–CO_2 interaction is much smaller than the CO_2–surface interaction. The attractive potentials due to the overlap of the pore walls is most significant in the smallest pore, resulting in deep energy wells associated with these systems. In the larger pores, due to the weak interactions of the neighboring pore walls, the CO_2–CO_2 interactions dictate the adsorption. The packing efficiency of bulk-phase CO_2 is lower than the adsorbed condensed-phase CO_2, and thus the overall densities decrease with increasing pore diameter. At higher loadings, e.g., 30 MPa of CO_2, the adsorption region near the pore walls is saturated, and the CO_2 molecules are compressed within the central region of the pores. With an increase in pore width, the fraction of the condensed adsorption layer decreases, and the overall changes of densities do not change significantly.

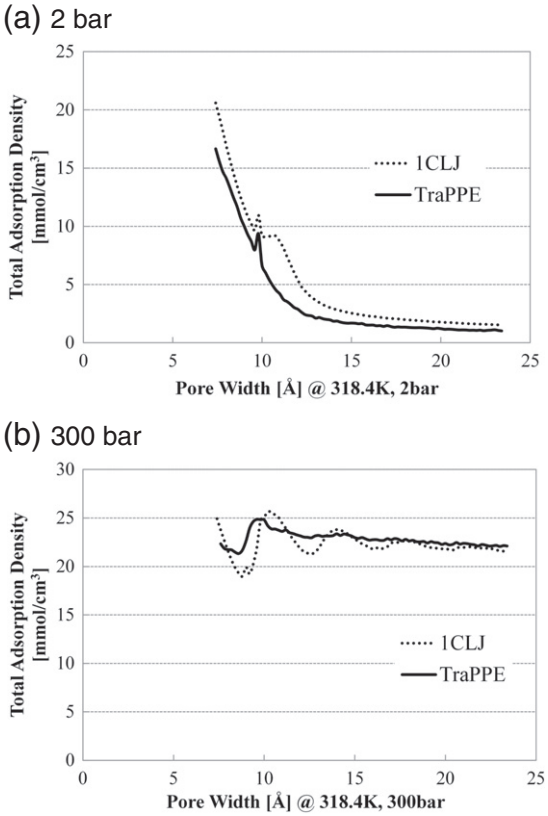

Fig. 2. Comparison of the total loading as a function of the pore width by using two different potential models of CO_2.

Fig. 2 also shows the comparisons of the total amount of CO_2 in the slit pores per unit volume as a function of the pore width using two different potential models. The overall trends of the average CO_2 densities simulated by the two models are the same, while the TraPPE model shows less fluctuation of the density change with an increase in pore diameter, thereby representing more accurately a real system. Due to the fact that the continuous increase of the pore width does not result in the continuous increase of new CO_2 layers, where CO_2 exists either in the condensed phase or in the bulk fluid phase, especially when the pore size is small, the density change is not monotonic. When the TraPPE model is employed, the orientation changes of the CO_2 molecules are captured, allowing CO_2 to reach a maximum packing efficiency, and hence, the density change is smoother as a function of pore size.

3.1.2. Effects of pore size on CO_2 adsorption

When CO_2 in the micro- and meso-pore spaces is equilibrated with the bulk phase, CO_2 that is close to the pore walls has enhanced interaction with the surfaces and, thus, is bound as significantly condensed phase. Due to the overlapping potentials associated with the strong CO_2–wall and CO_2–CO_2 interactions, the CO_2 density close to the surface is higher than that of fluid density in the center of the pore. In the center region of the pore, the CO_2 molecules are far enough from the pore surfaces that CO_2–CO_2 interactions dominate the phase behavior, with resulting CO_2 densities approximately equal to that of the bulk fluid. Therefore, the CO_2 density distribution in the micro- and mesopores is not homogeneous. To investigate the general effect of pore size on adsorption, the 1C-LJ model was employed, and the local CO_2 density distribution is plotted as a function of pore size as shown in Fig. 3. Surface occupancy in moles per unit surface area has been investigated to represent the local density of CO_2 in the different regions of a given pore. As shown in Fig. 3, the

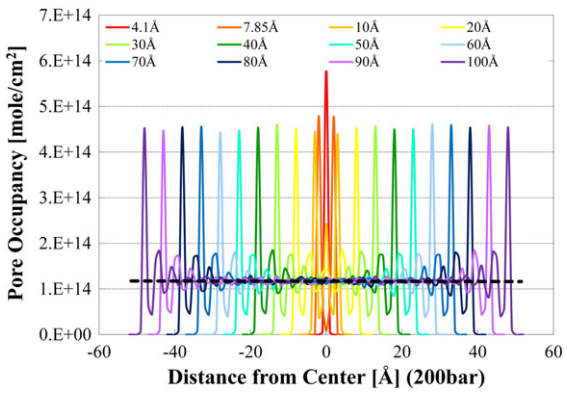

Fig. 3. Effect of pore size on the CO_2 density distribution.

CO_2 densities near pore walls are higher than in the pore center. In the smaller pores, i.e., ultramicropores (average pore diameter of less than 7 Å as defined by IUPAC (Sing et al., 2008)), due to the extra strong pore wall–wall interaction, the condensed adsorbed-CO_2 density is even higher than that of the larger pores. It has also been observed that the influence of the width of the bulk CO_2 phase in the pore center is negligible on the densities of the CO_2 adsorbed close to the pore walls.

3.1.3. Prediction of the CO_2 adsorption isotherm and pore size distribution (PSD) for an activated carbon (AC) sample

Predicted excess adsorption isotherms of CO_2 from molecular simulation are compared to experimental excess adsorption isotherms on an activated carbon sample (Filtrasorb 400, mesh 12×40, Batch Nr. FE 90623B) sourced from Chemviron Carbon (Neu-Isenburg, Germany) at supercritical and near-critical conditions (Pini et al., 2006) with a known PSD. To this aim, the experimentally measured pore size distribution was truncated to include only the micropore and lower mesopore range since it is likely that for the density of CO_2 in pores greater than 20 nm, the density can simply be estimated as that of the bulk-phase CO_2 at the same temperature and pressure conditions. Based on the assumption that the real porous system is a linear combination of slit pores with varying widths, the predicted excess adsorption isotherm is then calculated as the weighted average of the excess isotherms obtained from density estimates of single pores at the various sizes of the PSD. Conversely, the pore size distribution (PSD) can be determined by fitting the computed adsorption isotherm to the experimental measurement, provided that the adsorption isotherm data is available.

In the case that the PSD is provided, the adsorption isotherm can be predicted. As shown in Fig. 4(a), the PSD was measured for activated carbon Filtrasorb 400 sample, and PSD was truncated due to the fact that pore-filling rather than gas adsorption dictates the gas storage process in larger pores with negligible excess adsorption. The PSD was truncated at 20 nm and normalized as shown in Fig. 4(b). The simulated adsorption isotherm is calculated by:

$$\rho_{simulated}(j) = \sum_{i=1}^{m} a_i \rho_i(j) \tag{2}$$

such that a_i is the fraction of pores with corresponding widths. The set of isotherms for a given system were obtained from GCMC simulations.

Fig. 4(c) shows the comparison of the simulated adsorption isotherm and the measured adsorption isotherm of the given PSD. The simulated adsorption isotherm is consistent with the lab measurement, especially in the low-pressure region. At high-pressure conditions, the molecular simulation results underpredict the adsorption. There are several possible reasons for these discrepancies. The first

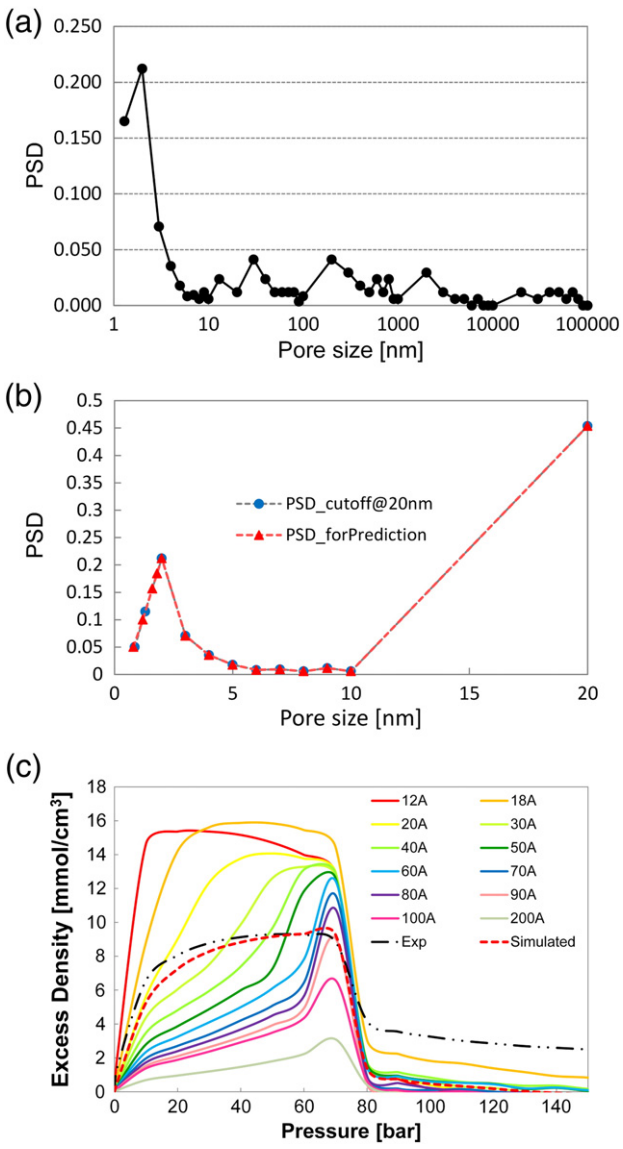

Fig. 4. (a) Measured PSD for activated carbon sample Filtrasorb 400; (b) PSD cutoff at 20 nm for simulation; (c) Comparison of the simulated adsorption isotherm with the experimental measurement at 305 K.

is due to the fact that the real organic pore structures of AC are more complex than the simplified perfect graphite slit-pore model, which includes highly structural and chemical heterogeneities that may enhance (or hinder) CO_2 adsorption. For instance, the model predictions do not allow swelling or expansion of the pore walls, which coal has exhibited. Since the AC is sourced from carbon, it may be possible that this swelling effect may occur to some extent. (Jiang et al., 1994) The second reason is that the measured PSD does not account for the complete pore structure since micropores, which are classified as smaller than 2 nm, cannot be measured accurately using nitrogen as a probe gas. Including the full extent of the micropores, and in particular ultramicropores, is essential for accurate measurements and subsequent pore capacity predictions. As mentioned previously, CO_2 may see pore sizes smaller than the probe gas, nitrogen, and this could lead to potential discrepancies between the predictions and the measurements, as the CO_2 density and relative capacity increases significantly with decreasing pore size.

Conversely, in the case that the adsorption isotherm is measured, and the PSD is required, a least-squares problem was solved with two constraints. As shown in Fig. 5(b), the predicted PSD is compared to

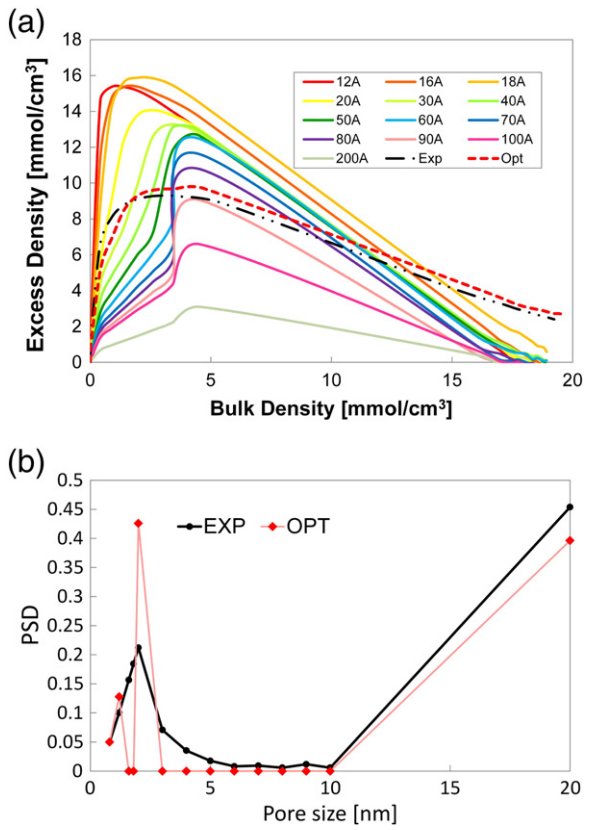

Fig. 5. Optimization of PSD based on the measured adsorption isotherm. (a) Comparison between the optimized excess density predictions of Eq. (3) to the adsorption measurements. (b) Comparison between the predicted PSD from the linearized coefficients of Eq. (3) to the measured PSD.

the measured PSD for activated carbon Filtrasorb 400. Most of the pores that are smaller than 200 nm are concentrated near 2 nm, which is consistent with the measurement.

$$\text{Total Error} = \sum_{j=1}^{n}\left[\sum_{i=1}^{m} a_i\rho_i(j) - \rho_{exp}(j)\right]^2 = \min \tag{3}$$

$$\text{Constraint 1: } \sum_{i=1}^{m} a_i = 1$$

$$\text{Constraint 2: } a_i \geq 0$$

such that the coefficients a_i correspond to the fraction of each pore.

3.2. Bader charge analysis of the perfect and functionalized graphitic surfaces

To investigate the effect of surface functionality of carbons, the partial charge distribution of the pore surfaces is essential.

3.2.1. Bader charge analysis of the hydrated graphite surface

In the current work, the two most stable configurations of dissociated H_2O suggested by Kostov et al. (2005) and one configuration of dissociated CO_2 (Liu and Wilcox, 2011) on the mono-vacancy site of a 3-layer graphite slab have been investigated. The hydrated graphitic surfaces have calculated zero-pressure zero-temperature adsorption energies of approximately −102 kcal/mol and −91 kcal/mol, respectively, using the DFT-D methodology compared to estimates of −87 kcal/mol and −76 kcal/mol, which were reported for dissociated H_2O on the mono-vacancy site of graphene (Kostov et al., 2005). The reason for the lower predicted adsorption energies of the previous work is due to the different reference point chosen by Kostov et al. (2005), who chose the relaxed physisorbed water molecule over the center of the vacancy as the energy reference. Compared to dissociated H_2O at the mono vacancy defect site, CO_2 has a higher adsorption energy (i.e., −42 kcal/mol) and, thus, is less stable. The optimized geometries of these three configurations are available in the Supplementary data. At a given pressure and temperature, the mono-vacancy defect site with dissociated H_2O yields a lower surface free energy; therefore, H_2O dissociation is more likely than CO_2 dissociation or chemisorption.

Fig. 6 shows the results of a Bader charge analysis of the most stable hydrated graphite surface carried out in the current work. For atoms that have a higher electron density compared to the original neutral atom, the negative partial charge values represent an electron gain from the other surface atoms. These electronegative atoms have an increased potential to electron donation to the gas-phase molecules in the pore space, such as CO_2 in this case. Therefore, as Fig. 6 indicates, the oxygen atom is highly electronegative, and thus can serve as a basic adsorption site on the basal plane. The partial charge values calculated based on the DFT-D method were compared with the results of the electronic structure calculations without the *van der Waals* correction. The maximum difference in the charge associated with the top-layer atoms is lower than 1%, which minimally impacts the GCMC simulations. Therefore, the corrections were neglected for the GCMC simulations. Due to the balanced computational efficiency and reasonable accuracy, the Bader charge results based on the DFT calculations were employed in the molecular simulations.

3.2.2. Bader charge analysis of the oxygen-containing functionalized graphite surface

With the exception of the functional groups formed due to the competition of volatile components, such as H_2O as discussed in the previous section, the partial charge distribution of the embedded oxygen-containing functional groups has also been considered. Similar to hydrated graphite surfaces with dissociated H_2O at the mono-vacancy defect site, the embedded oxygen atoms on each surface also exhibit high electronegativities due to electron gain from the surrounding surface carbon atoms. For example, oxygen contained within a carbonyl functional group has a partial charge of −1.047e, and, therefore, has the highest potential among all the surface atoms to donate electrons to the neighboring gas molecules. Within these scenarios, oxygen-containing functional groups seem to allow for enhanced electron transport and versatility depending on the acid–base nature of the adsorbate, with oxygen atoms acting as a Lewis base donating their electron density to the acidic carbon atoms of CO_2 molecules. Due to the higher electronegativities of the O atoms than the C atom of CO_2 molecules, the C atom will be more attracted to the embedded oxygen functional groups. It is expected that the packing pattern of the adsorbed CO_2 molecule will be influenced by this interaction and the CO_2 adsorption will be enhanced or passivated by the presence of embedded oxygen functional groups. The overall results of the Bader charge analyses for all of the functionalized surfaces investigated are shown in Fig. 7. Based on the Bader charge analyses, graphitic slit pores with embedded hydroxyl and carbonyl functional groups are hypothesized to more strongly influence surface–CO_2 interactions compared to the other functional groups investigated.

3.3. Adsorption of CO_2 within perfect and functionalized slit-pores

3.3.1. Pore volume of the oxygen-containing functionalized slit pores

The unit cell volumes of the micropores with the same pore width have been compared. All of the pore volumes have been normalized to the perfect graphite slit pores with the corresponding pore width. For pores approximately 9.2 Å and 20 Å wide, it is important to note that the actual pore volume varies due to the different geometries of the functional groups present, even though the pore widths themselves are equal. For example, compared to the slit pore with a perfect graphite

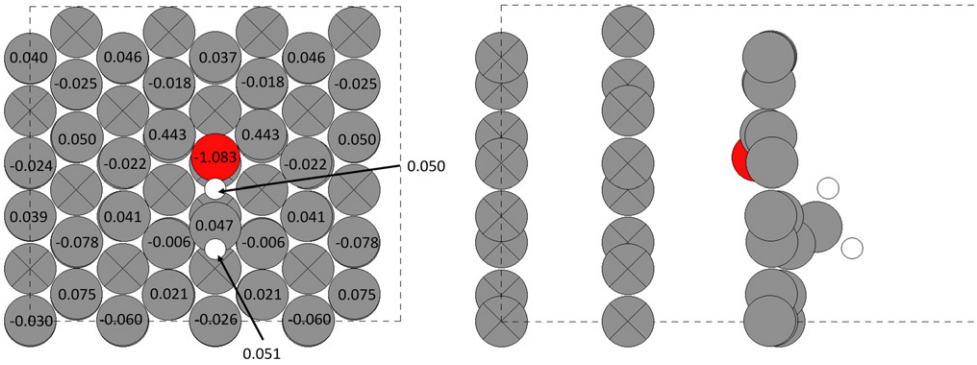

Fig. 6. Partial charge distribution of a hydrated graphitic surface (i.e., dissociated H_2O on the mono-vacancy site of the top layer of graphite). Left: top view; Right: side view. Gray, carbon atoms (cross represents bottom two layers); red, oxygen atom; white, hydrogen atoms.

surface, a hydroxyl functional group embedded in the top layer of the graphite surface in a 9.2 Å pore decreases the volume by approximately 40%. Fig. 8 shows a complete comparison of pore volumes with different surface functionalities for both 9.2 Å and 20 Å pores.

3.3.2. CO_2 adsorption in the oxygen-containing functionalized slit pores

Fig. 9 shows a comparison of CO_2 adsorption isotherms for different functionalized graphitic slit pores at two different temperature conditions corresponding to carbon storage applications. The loading

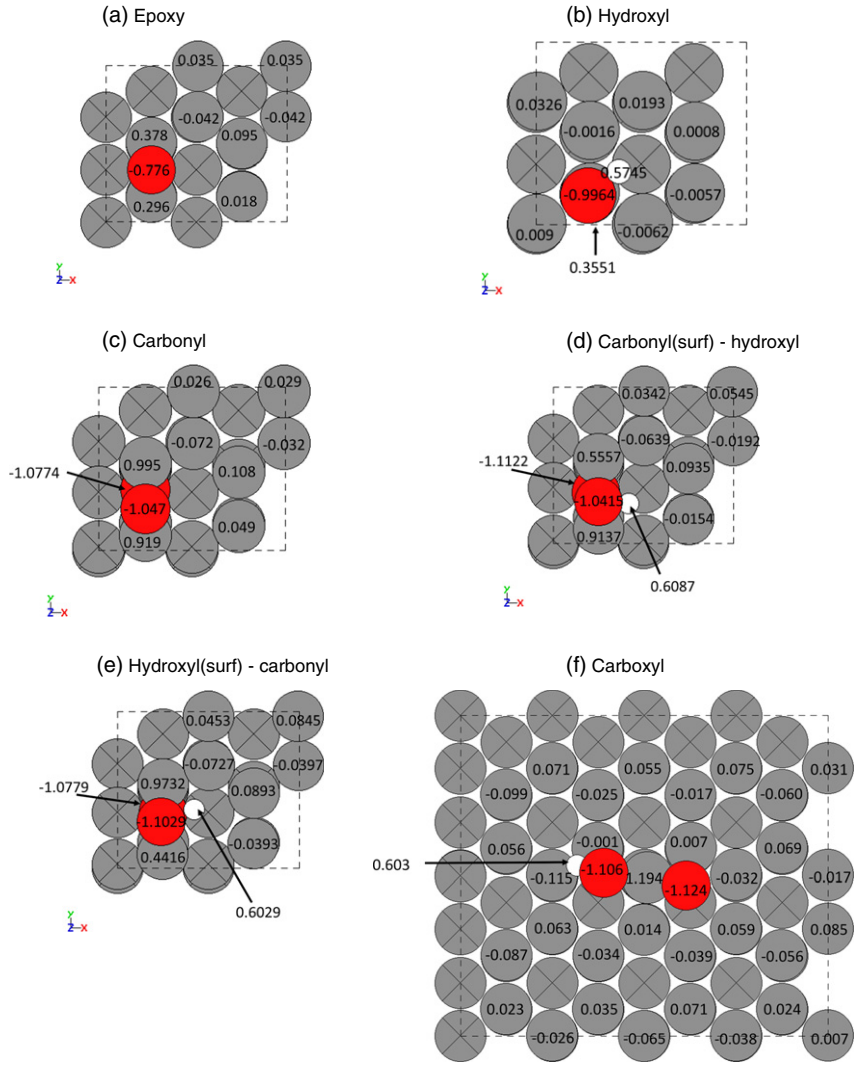

Fig. 7. Partial charge distributions of various oxygen-containing functionalized graphite surfaces. Gray, carbon atoms (cross represents bottom two layers); red, oxygen atom; white, hydrogen atoms.

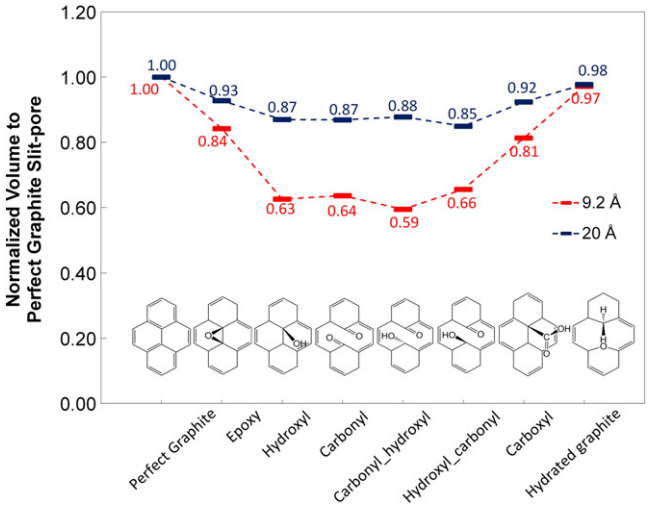

Fig. 8. Comparison of the pore volumes with different surface functionalities.

represents the total amount of CO_2 (including CO_2 in both condensed surface-bound and gas phases) per unit pore volume. In micropores such that the diameter is less than 2 nm (Sing et al., 2008), adsorption is governed by CO_2–surface interactions with wall–wall interactions also playing a significant role. In general, the oxygen-containing functional groups increase the adsorbed CO_2 density in micropores, especially in the cases of hydroxyl = and carbonyl-functionalized graphitic slit pores. These results are consistent with the electronic structure predictions, in that the higher electron densities surrounding the oxygen atoms of functional groups attract more CO_2.

To further explore the packing configurations of adsorbed CO_2, the local adsorbed CO_2 densities at different CO_2 orientations were compared among different investigated embedded functional groups, as shown in Fig. 10. In the perfect graphite slit pore the CO_2 molecules are aligned mostly parallel to the pore surfaces. In the 9.2-Å pores, due to the overlapping potentials from the strong pore wall–wall interations, the carbonyl functional group on the surface influences the CO_2 orientation profile significantly, with the majority of the CO_2 molecules oriented perpendicular to the surface. However, in the case of the surface functionalized with hydroxyl groups, the CO_2 molecules are oriented at approximately 30° or less with respect to the pore wall. Similarly, in the 20-Å pores, due to the weaker surface–surface interactions, the majority of the CO_2 molecules are rotated approximately 60° with respect to the surface with carbyonyl functional groups and are orientated at approximately 30° to the surface with hydroxyl functional groups upon adsorption. The functionality-induced packing pattern makes it more efficient for CO_2 to occupy the limited pore space, with this change in packing configuration allowing for enhanced CO_2 adsorption capacity in the slit pores with hydroxyl and carbonyl functional groups than without.

To have an improved understanding of the CO_2 packing, packing configuration snapshots of CO_2 in the functionalized graphitic surfaces at 25 MPa are shown in Fig. 11. Linear CO_2 molecules are represented by the red line segments. The CO_2 molecules are more organized and aligned when they are adsorbed in the functionalized slit pores, and, thus, the adsorption capacity is enhanced by the higher efficient side-by-side packing.

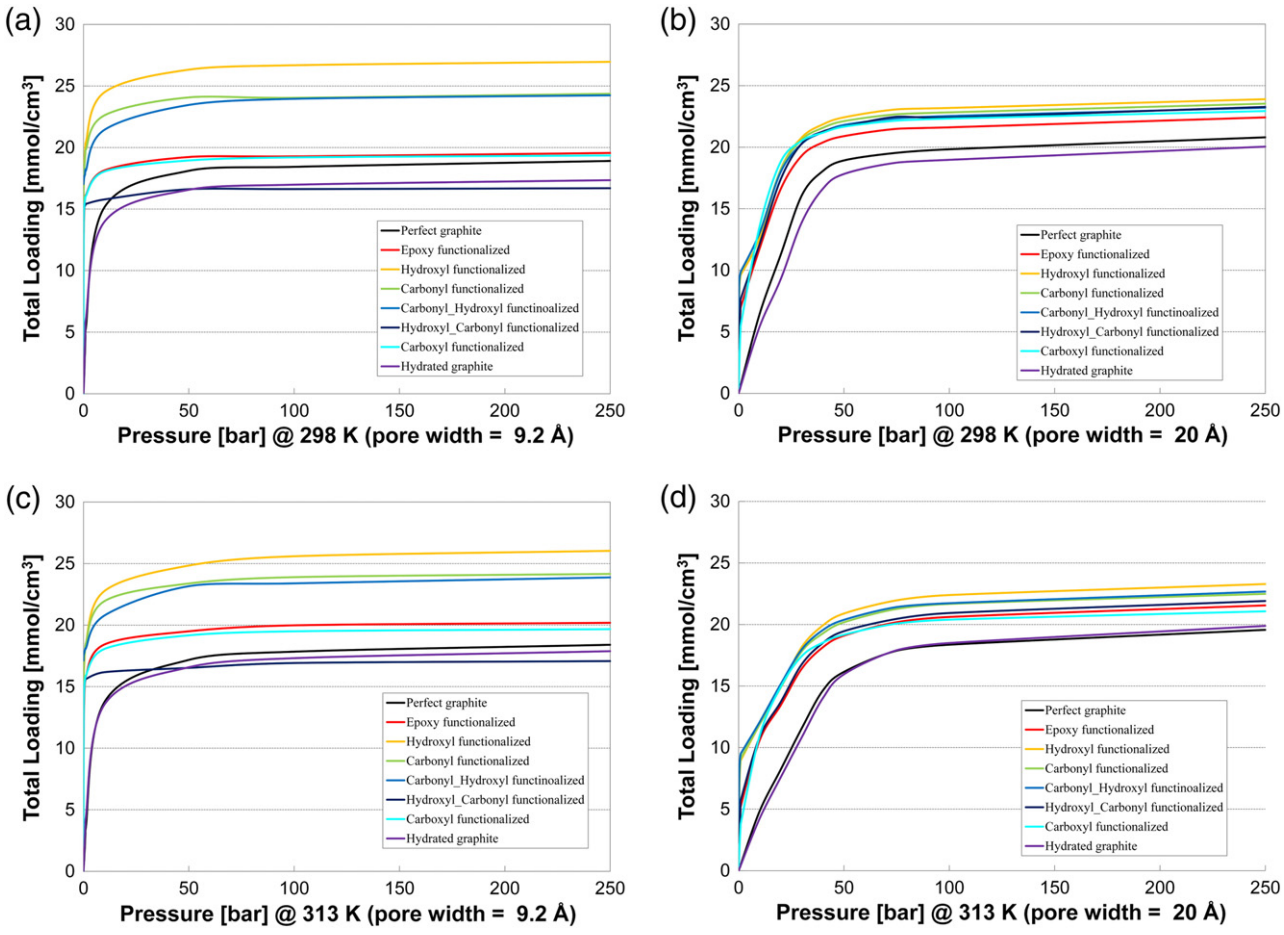

Fig. 9. Comparison of CO_2 adsorption isotherm in slit pores with different embedded surface functional groups.

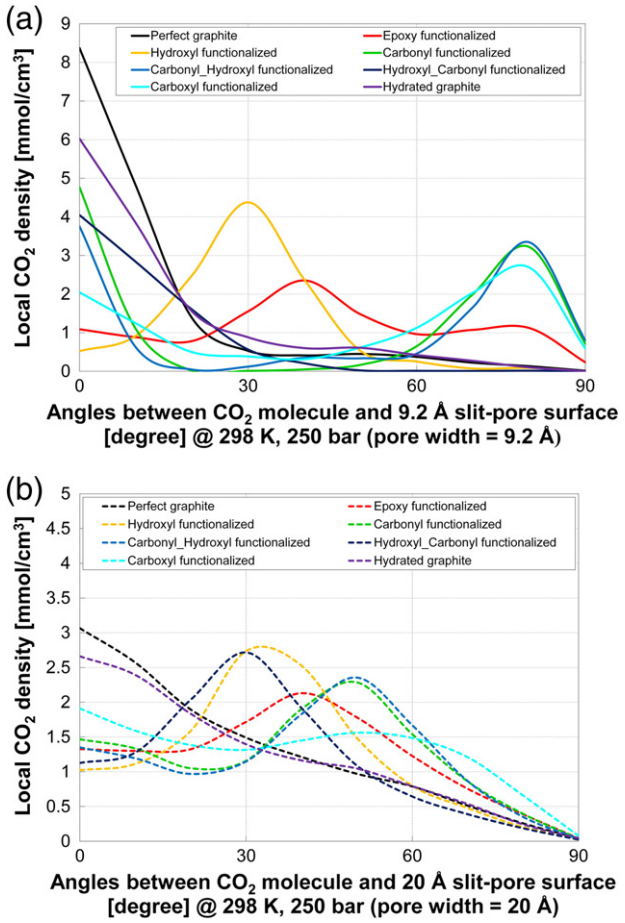

Fig. 10. Orientation distribution of CO_2 within functionalized micropores.

In the ultramicropores, due to the overlapping potentials from the strong pore wall–wall interactions and the strong CO_2–wall interaction, the CO_2 density of the condensed phase is even higher than that of the larger pores. In general, as the pore width decreases, the surface functionalities dictate the adsorption, and thus the surface functionalities play more of a role in enhancing the CO_2 adsorption capacity. The surface heterogeneity changes the adsorbates' accumulation configuration by changing the geometry of the pore surface and the charge distribution of the surface, which is consistent with the Bader charge results of the DFT study.

3.4. Estimation of the capacity of carbon storage in coal and shale reservoirs

In the case of CO_2 storage in unmineable coalbeds in the U.S., the current estimated CO_2 storage capacity is approximately 59 to 117 Gt (NETL, 2010). The typical approach to estimate the capacity of CO_2 storage resource potential is based on the static volumetric method without taking any coal chemical heterogeneity into account. The volumetric equation typically used to calculate the CO_2 storage resource mass (G_{CO2}) for geologic storage in unmineable coal areas is:

$$G_{CO_2} = A\, h_g C_{s,max} \rho_{CO_2,std} E_{coal} \tag{4}$$

such that A is the total area and h_g is the gross area thickness, both of which are associated with the coalbed for intended sequestration. $C_{s,max}$ is the maximum volume of CO_2 at standard conditions that can be adsorbed per volume of coal, which varies according to different coal seams, and can be simply predicted by the Langmuir isotherm volume constant along with available field data. $\rho_{CO2,std}$ is the CO_2 density at standard condition, which is used to convert CO_2 volume to mass. The storage efficiency factor E_{coal} ranges from 21 to 48% for coal, and reflects the fraction of the total bulk coal volume that will store the injected CO_2.

By taking surface functionality into account, the parameters in Eq. (4) for estimating the potential of CO_2 storage in coal will not be influenced except for the Langmuir isotherm volume constant $C_{s,max}$, which is the maximum extent of CO_2 at standard conditions that can be adsorbed per volume of coal. Within molecular simulation, without fitting field data to the Langmuir isotherm to investigate the change of $C_{s,max}$ directly, the average CO_2 density in the functionalized slit pores were investigated.

Fig. 12 shows the local density distribution of CO_2 in the investigated functionalized slit pores with different pore widths at conditions of 298 K and 25 MPa. The bulk CO_2 density at the same pressure and temperature is also illustrated in all of the figures, in addition to the density of dry ice, which is perceived to be the most efficient packing of CO_2. Both the bulk CO_2 density and dry ice density are homogeneous in the pore space; however, the local density distributions of CO_2 in the slit pores are far from uniform. In the case of the 9.2 Å pores, due to the overlap of the strong surface–surface and the CO_2–surface interactions, the condensed phases of CO_2 are concentrated in the middle of the pores, with an even higher density than that of bulk CO_2 or dry ice. In the case of the wider pores, e.g., 20-Å pores, the influence of the surface–surface interactions is weaker, and CO_2 is more layered and uniformly distributed as shown in Fig. 11. The CO_2 density is high near the pore walls, and is close to the bulk density in the middle of the pores.

In reality, the local CO_2 density distribution is difficult to measure. In addition, the overall average CO_2 density in the slit pores with different surface functionalities further complicates the adsorption mechanism, but is important for an accurate prediction of the CO_2 storage capacity. To investigate the effect of surface chemistry on the CO_2 density, the total amount of CO_2 per unit volume is compared among perfect and functionalized slit pores, as shown in Tables 2 and 3 for different temperatures. Compared with the perfect graphite slit pore, the overall CO_2 density increases when CO_2 is adsorbed within the epoxy, hydroxyl, carbonyl, carbonyl_hydroxyl, and carboxyl functionalized slit pores. For example, at 298 K, in the case of 9.2-Å pores, hydroxyl-functionalized pore walls enhance the CO_2 density the most, with an increase greater than 40%. In the case of 20-Å pores, hydroxyl- and carbonyl-functionalized slit pores influence the CO_2 density the most, with density increases greater than 15%. Based on the GCMC simulation analysis, the homogeneous slit-pore model generally underpredicts the potential of CO_2 storage in coal, especially when hydroxyl and carbonyl functionalities are not negligible. It should be noted that, since the slit-pore model with surface functionality is an idealized model for coal and gas shale systems and that the coverage of surface functional groups was not taken into account in the current work, the increase in CO_2 density in the modeled systems is an approximation and will be investigated further in future work.

4. Summary

In the current work, DFT calculations have been performed to investigate the electronic properties of graphitic surfaces representative of the pores of coal and organic matrix of gas shale. Oxygen-containing functional groups suggested by previous researchers have been investigated in the current work. Charge analysis has been carried out to generate the partial charge distribution of the more realistic models of defective graphitic surfaces or surface-embedded functional groups. Grand canonical Monte Carlo simulations are carried out to simulate adsorption with different potential models for CO_2 to calculate accurate fluid–fluid and fluid–wall interactions. The implementation of the GCMC method yields the adsorption isotherms for a given adsorbent–

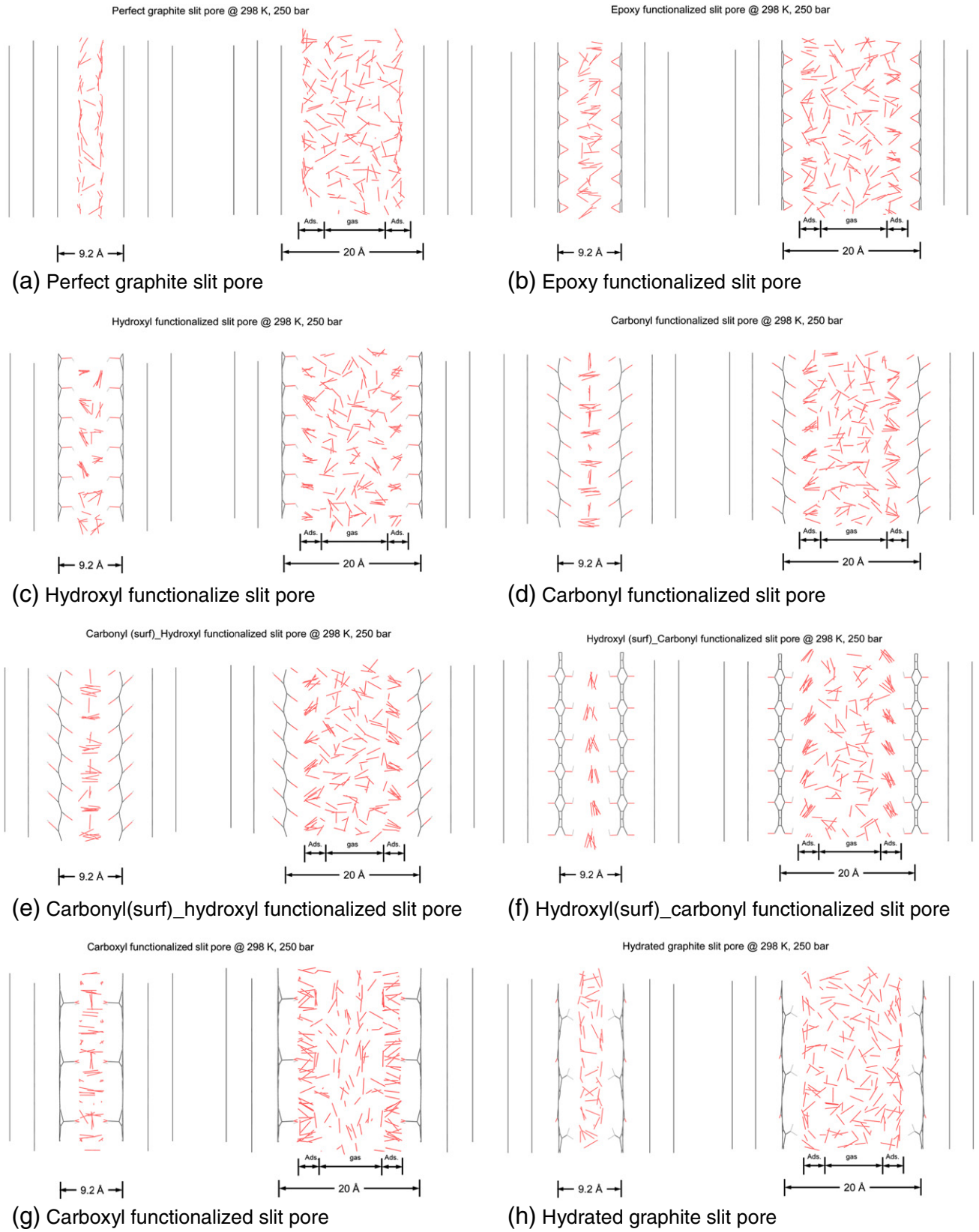

Fig. 11. Packing configurations of CO_2 in functionalized micropores. Left: side views of adsorbed CO_2 in various functionalized graphite slit pores with the pore width of 9.2 Å; Right: side views of adsorbed CO_2 in various functionalized graphite slit pores with the pore width of 20 Å.

adsorbate interaction. The effects of surface heterogeneity have been investigated, and it was found that functional groups with oxygen can enhance the adsorption of CO_2, hydroxyl functional groups, in particular.

The combination of DFT and GCMC simulation makes it possible to take the volatile components inherent within the pore structure into account. The dissociation of water vapor on the mono-vacancy site

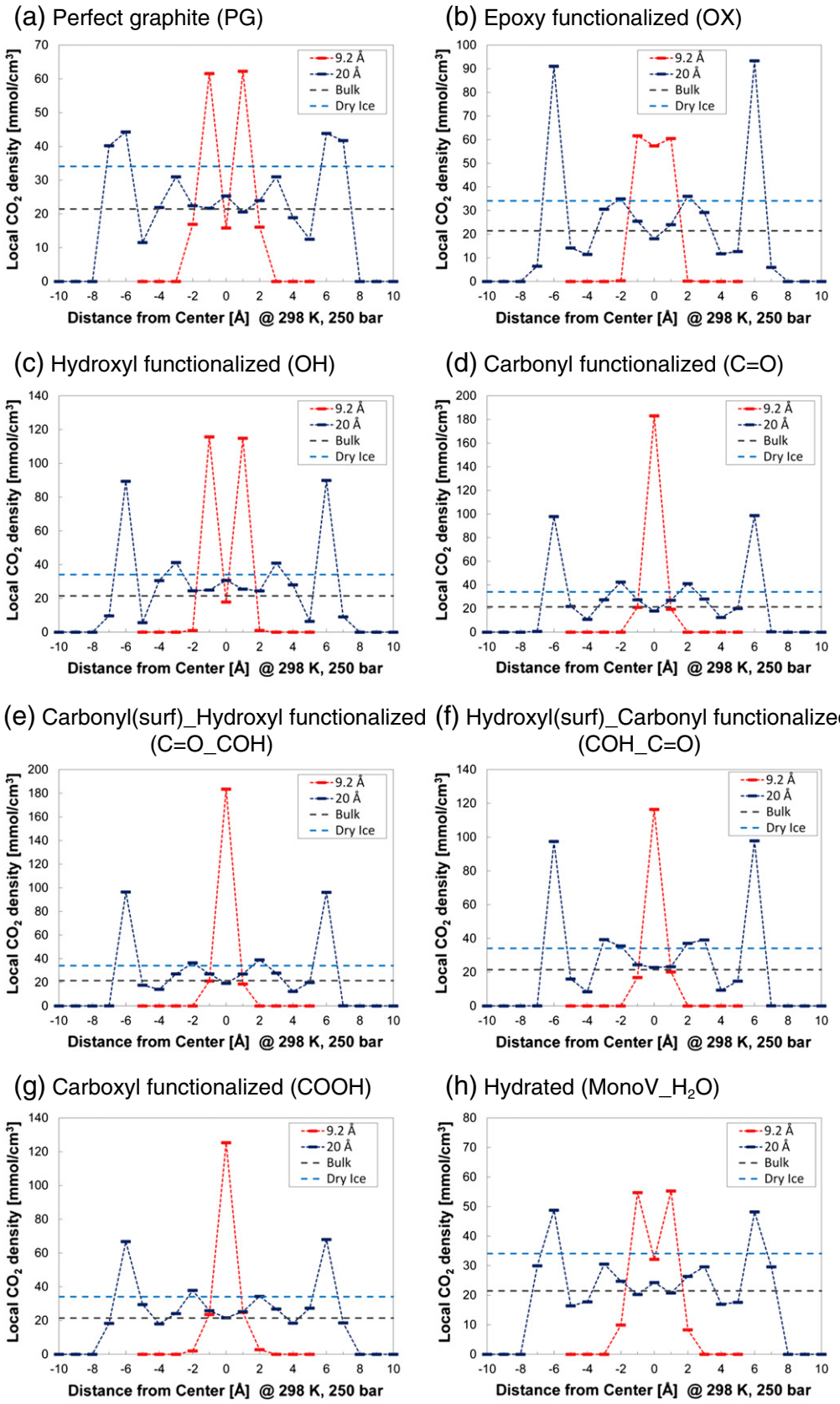

Fig. 12. Local CO_2 density distribution in various functionalized slit pores of two widths: 9.2 Å and 20 Å.

and the existence of various oxygen-containing functional groups result in the redistribution of partial charge and reconfiguration of surface geometry, leading to significant changes in the adsorbate–adsorbent interactions. With the consideration of surface chemistry, CO_2 storage capacity estimations in organic matrix of coal and gas shale increase when CO_2 is adsorbed in the micropores.

Table 2
CO_2 density in different functionalized slit pores at 298 K.

		PG	OX	OH	C═O	C═O_COH	COH_C═O	COOH	Hydrated
9.2 Å	Avg. density [mmol/cm^3]	18.76	19.55	27.20	24.28	24.24	16.67	19.40	17.42
	Increase [%]	0.00	4.22	44.99	29.41	29.21	−11.15	3.41	−7.13
20 Å	Avg. density [mmol/cm^3]	20.53	22.25	24.03	23.68	23.01	23.25	23.04	20.08
	Increase [%]	0.00	8.37	17.05	15.36	12.06	13.24	12.23	−2.19

Table 3
CO_2 density in different functionalized slit pores at 313 K (supercritical).

		PG	OX	OH	C═O	C═O_COH	COH_C═O	COOH	Hydrated
9.2 Å	Avg. density [mmol/cm3]	18.53	20.15	26.22	23.86	23.86	17.01	19.40	17.90
	Increase [%]	0.00	8.78	39.77	27.21	27.21	−9.36	3.41	−4.61
20 Å	Avg. density [mmol/cm3]	19.41	21.34	23.17	22.56	22.57	21.82	21.05	19.83
	Increase [%]	0.00	9.93	19.36	16.21	16.26	12.42	8.42	2.14

Acknowledgments

This research is funded by a BP PhD Fellowship through the School of Earth Sciences at Stanford University. We thank Dr. Anthony Kovseck, Dr. Mark Zoback, and Dr. Ronny Pini for their helpful discussions and insight regarding this work. The computations were carried out on the Center for Computational Earth & Environmental Science (CEES) cluster at Stanford University. We also thank our cluster administrator, Dennis Michael for installation of MUSIC and VASP on the CEES cluster.

Appendix A. Supplementary data

Figure S1 provides the optimized geometries of H_2O and CO_2 dissociation on the mono-vacancy site of the top layer of a graphite slab. Details of the prediction of pore volume from the helium adsorption second virial coefficient in addition to a comparison of the real pore volumes with different surface functionalities are available in the Supplementary Data. Supplementary materials related to this article can be found online at doi:10.1016/j.coal.2012.04.007.

References

Allen, M.P., Tildesley, D.J., 1989. Computer Simulation of Liquids. Clarendon Press, Oxford.
Allouche, A., Ferro, Y., 2006. Dissociative adsorption of small molecules at vacancies on the graphite (0001) surface. Carbon 44, 3320–3327.
Bader, R.F.W., 1990. Atoms in Molecules: A Quantum Theory. Oxford University Press, New York.
Bagri, A., Grantab, R., Medhekar, N.V., Shenoy, V.B., 2010. Stability and formation mechanisms of carbonyl- and hydroxyl-decorated holes in graphene oxide. Journal of Physical Chemistry C 114, 12053–12061.
Benson, S., Cook, P., 2005. Underground Geological Storage. Intergovernmental Panel on Climate Change, Special Report on Carbon dioxide Capture and Storage, Chapter 5. Cambridge University Press, Cambridge, UK.
Bhatia, S.K., Tran, K., Nguyen, T.X., Nicholson, D., 2004. High-pressure adsorption capacity and structure of CO_2 in carbon slit pores: theory and simulation. Langmuir 20, 9612–9620.
Cabrera-Sanfelix, P., 2009. Adsorption and reactivity of CO_2 on defective graphene sheets. Journal of Physical Chemistry A 113 (2), 493–498.
Chen, L., Johnson, J.K., 2005. Formation of odd-numbered clusters of CO_2 adsorbed on nanotube bundles. Physical Review Letters 94 (12), 125701.
Cinke, M., Li, J., Bauschlicher, C.W., Ricca, A., Meyyappan, M., 2003. CO_2 adsorption in single-walled carbon nanotubes. Chemical Physics Letters 376, 761–766.
Frenkel, D., Smit, B., 2002. Understanding Molecular Simulation, 2nd ed. Academic Press, San Diego.
Grimme, S., 2006. Semiempirical GGA-type density functional constructed with a long-range dispersion correction. Journal of Computational Chemistry 27, 1787–1799.
Gupta, A., Chempath, S., Sanborn, M.J., Clark, L.A., Snurr, R.Q., 2003. Object-oriented programming paradigms for molecular modeling. Molecular Simulation 1 (29), 29–46.
Haenel, M.W., 1992. Recent progress in coal structure research. Fuel 71, 1211–1223.
Hashimoto, A., Suenaga, K., Gloter, A., Urita, K., 2004. Direct evidence for atomic defects in graphene layers. Nature 430 (19), 870–873.
Hu, X., Radosz, M., Cychosz, K.A., Thommes, M., 2011. CO_2-filling capacity and selectivity of carbon nanopores: synthesis, texture, and pore-size distribution from quenched-solid density functional theory (QSDFT). Environmental Science and Technology 45 (16), 7068–7074.
Jiang, J.W., Sandler, S.I., 2005. Separation of CO_2 and N_2 by adsorption in C168 Schwarzite: a combination of quantum mechanics and molecular simulation study. Journal of the American Chemical Society 127, 11989–11997.
Jiang, S.Y., Zollweg, J.A., Gubbins, K.E., 1994. High-pressure adsorption of methane and ethane in activated carbon and carbon fibers. Journal of Physical Chemistry 98, 5709–5713.
Jorge, M., Schumacher, C., Seaton, N.A., 2002. Simulation study of the effect of the chemical heterogeneity of activated carbon on water adsorption. Langmuir 18 (24), 9296–9306.
Kostov, M.K., Santiso, E.E., Gubbins, K.E., Nardelli, M.B., 2005. Dissociation of water on defective carbon substrates. Physical Review Letters 95, 136105.
Kowalczyk, P., Furmaniak, S., Gauden, P.A., Terzyk, A.P., 2010. Carbon dioxide adsorption-induced deformation of microporous carbons. Journal of Physical Chemistry C 114, 5126–5133.
Kresse, G., Furthmüller, J., 1996. Efficiency of ab initio total energy calculations for metals and semiconductors using a plane-wave basis set. Computational Materials Science 6, 15–50.
Kresse, G., Hafner, J., 1993. Ab initio molecular dynamics for open-shell transition metals. Physical Review B 48, 13115–13118.
Kresse, G., Joubert, D., 1999. From ultrasoft pseudopotentials to the projector augmented-wave method. Physical Review B 59, 1758–1775.
Kudin, K.N., Ozbas, B., Schniepp, H.C., Prud'homme, R.K., Aksay, I.A., Car, R., 2008. Raman spectra of graphite oxide and functionalized graphene sheets. Nano Letters 8 (1), 36–41.
Kurniawan, Y., Bhatia, S.K., Rudolph, V., 2006. Simulation of binary mixture adsorption of methane and CO_2 at supercritical conditions in carbons. AICHE Journal 52 (3), 957–967.
Lastoskie, C., Gubbins, K.E., Quirket, N., 1993. Pore size heterogeneity and the carbon slit pore: a density functional theory model. Langmuir 9, 2693–2702.
Liu, Y., Wilcox, J., 2011. CO_2 adsorption on carbon models of organic constituents of gas shale and coal. Environmental Science and Technology 45 (2), 809–814.
Matranga, C., Chen, L., Smith, M., Bittner, E., Johnson, J.K., Bockrath, B., 2003. Trapped CO_2 in carbon nanotube bundles. The Journal of Physical Chemistry. B 107, 12930–12941.
Matranga, C., Chen, L., Bockrath, B., Johnson, J.K., 2004. Displacement of CO_2 by Xe in single-walled carbon nanotube bundles. Physical Review B 70 (165416), 1–7.
Melnichenko, Y.B., Radlinski, A.P., Mastalerz, M., Cheng, G., Rupp, J., 2009. Characterization of the CO_2 fluid adsorption in coal as a function of pressure using neutron scattering techniques (SANS and USANS). International Journal of Coal Geology 77, 69–77.
Monkhorst, H.J., Pack, J.D., 1976. Special points for Brillouin-zone integrations. Physical Review B 13, 5188–5192.
Montoya, A., Mondragon, F., Truong, T.N., 2003. CO_2 adsorption on carbonaceous surface: a combined experimental and theoretical study. Carbon 41, 29–39.
Müller, E.A., 2005. Adsorption of super greenhouse gases on microporous carbons. Environmental Science and Technology 39 (22), 8736–8741.
National Energy Technology Laboratory, 2010. Carbon Sequestration Atlas of the United States and Canada — Third Edition (Atlas III). U.S. Department of Energy, Washington, DC.
Perdew, J.P., Burke, K., Ernzerhof, M., 1996. Generalized gradient approximation made simple. Physical Review Letters 77.
Pini, R., Ottiger, S., Rajendran, A., Storti, G., Mazzotti, M., 2006. Reliable measurement of near-critical adsorption by gravimetric method. Adsorption 12, 393–403.
Potoff, J., Siepmann, J., 2001. Vapor–liquid equilibria of mixtures containing alkanes, carbon dioxide and nitrogen. AICHE Journal 47, 1676–1682.
Radlinski, A., Busbridge, T.L., Blach, T.P., Gray, E. MacA, Chen, G., Melnichenko, Y.B., Cookson, D.J., Mastalerz, M., Esterle, J., 2009. Dynamic micro-mapping of CO_2 sorption in coal. Langmuir 25, 2385–2389.
Rivera, J.L., McCabe, C., Cummings, P.T., 2002. Layering behavior and axial phase equilibria of pure water and water + carbon dioxide inside single carbon nanotubes. Nano Letters 2, 1427–1431.
Sanfelix, P.C., Holloway, S., Kolasinski, K.W., Darling, G.R., 2003. The structure of water on the (0 0 0 1) surface of graphite. Surface Science 532–535, 166–172.

Sing, K.S.W., Everett, D.H., Haul, R.A.W., Moscou, L., Pierotti, R.A., Rouquerol, J., Siemieniewska, T., 2008. Reporting physisorption data for gas/solid systems. Handbook of Heterogeneous Catalysis, pp. 1217–1230.

Smith, K.L., Smoot, L.D., Fletcher, T.H., Pugmire, R.J., 1994. The Structure and Reaction Processes of Coal. Plenum Press, New York.

Tenney, C.M., Lastoskie, C.M., 2006. Molecular simulation of carbon dioxide adsorption in chemically and structurally heterogeneous porous carbons. Environmental Progress 25 (4), 343–354.

U.S. Department of Energy, 2010. Basic Research Needs for Carbon Capture: Beyond 2020. Washington, DC. Available at: http://www.sc.doe.gov/bes/reports/files/CCB2020_rpt.pdf.

U.S. Energy Information Administration, 2012. Annul Energy Outlook 2012 Early Release. Washington, DC. Available at: http://www.eia.gov/forecasts/aeo/er/pdf/0383er(2012).pdf.

van Krevelen, D.W., 1991. Coal, 3rd Completely Revised Edition. Elsevier, Amsterdam, The Netherland.

White, C.M., Smith, D.H., Jones, K.L., Goodman, A.L., Jikich, S.A., LaCount, R.B., DuBose, S.B., Ozdemir, E., Morsi, B.I., Schroeder, K.T., 2005. Sequestration of carbon dioxide in coal with enhanced coalbed methane recovery—a review. Energy & Fuels 19, 659–724.

Wilcox, J., 2012. Carbon Capture. Springer, New York.

Xu, S.C., Irle, S., Musaev, D.G., Lin, M.C., 2006. Quantum chemical prediction of reaction pathways and rate constants for dissociative adsorption of CO_x and NO_x on the graphite (0001) surface. The Journal of Physical Chemistry. B 110 (42), 21135–21144.

Yim, W.L., Byl, O., Yates, J.T., Johnson, J.K., 2004. Vibrational behavior of adsorbed CO_2 on single-walled carbon nanotubes. Journal of Chemical Physics 120 (11), 5377–5386.

Zhao, J.J., Buldum, A., Han, J., Lu, J.P., 2002. Gas molecule adsorption in carbon nanotubes and nanotube bundles. Nanotechnology 13 (2), 195–200.

Zhu, D., Kwon, S., Pignatello, J.J., 2005. Adsorption of single-ring organic compounds to wood charcoals prepared under different thermochemical conditions. Environmental Science and Technology 39 (11), 3990–3998.